Energy Conversion and Management 74 (2013) 377–385

Contents lists available at SciVerse ScienceDirect

Energy Conversion and Management

journal homepage: www.elsevier.com/locate/enconman

CFD simulation of air to air enthalpy heat exchanger

Rafat Al-Waked [a,*], Mohammad Shakir Nasif [b], Graham Morrison [c], Masud Behnia [d]

[a] Mechanical Engineering Department, Prince Mohammad Bin Fahd University, AlKhobar, Saudi Arabia
[b] Mechanical Engineering Department, Universiti Teknologi PETRONAS (UTP), Perak, Malaysia
[c] School of Mechanical and Manufacturing Engineering, University of New South Wales, Sydney, Australia
[d] School of Aerospace, Mechanical and Mechatronic Engineering, University of Sydney, Sydney, Australia

ARTICLE INFO

Article history:
Received 16 February 2013
Accepted 29 May 2013

Keywords:
Energy recovery
CFD
Heat exchanger
Conjugate heat transfer
Membrane
Conjugate mass transfer

ABSTRACT

A CFD model which supports conjugate heat and mass transfer problem representation across the membrane of air-to-air energy recovery heat exchangers has been developed. The model consists of one flow passage for the hot stream and another for the adjacent cold stream. Only half of each flow passage volume has been modelled on each side of the membrane surface. Three dimensional, steady state and laminar flow studies have been conducted using a commercial CFD package. The volumetric species transport model has been adopted to describe the H_2O and air gas mixtures. Mesh dependency has been examined and followed by validation of the CFD model against published data. Furthermore, effects of flow direction at the inlet of the heat exchanger on its thermal effectiveness have been investigated. Simulation results are presented and analysed in terms of sensible effectiveness, latent effectiveness and pressure drop across the membrane heat exchanger. Results have shown that counter-flow configuration has greater sensitivity to the mesh centre perpendicular distance from the membrane when compared to the other two flow configurations (cross-/parallel-flow). However, the lateral mesh element length has shown minimal effect on the thermal effectiveness of the enthalpy heat exchanger. For the quasi-flow heat exchanger, a perpendicular flow direction to the inlets has been found to produce a higher performance in contrast to the non-perpendicular flow.

1. Introduction

Operating costs of air conditioning systems in commercial buildings are significant due to high HVAC total loads especially those built in tropical climate [1]. Of the total building energy consumption, the HVAC sector accounts for 33% [2,3]. Furthermore, total greenhouse gases (GHG) emissions from HVAC operations in residential and commercial buildings could account for 22% of the total GHG emissions [4]. Reducing the total HVAC load would result in a reduction in operating costs, GHG emissions and related environmental impacts [5].

Air-to-air fixed plate enthalpy/membrane heat exchanger is energy recovery equipment that provides energy savings and improved indoor air quality. Its energy recovering process is based on recovering heat and/or moisture from a stream at a high temperature and/or humidity and transferring the recovered energy to a low temperature and/or humidity stream. The effectiveness of exchanger depends heavily on air flow configurations, conditions and patterns of the supply and exhaust air streams. Designs that use cross-flow configuration or a combination of cross- and counter-flow (hybrid-flow) configuration, similar to the one shown by Fig. 1, are preferable. Noticeable advantages include high efficiency, ease of construction and no moving parts, has have made this type of exchanger popular for use in residential/commercial buildings [6–9].

In the mass transfer process, heat is released when the membrane absorbs moisture from the humid stream. The heat released transfers into the cold stream due to temperature discrepancy between the two streams. Similarly, the membrane desorbs moisture into the dry air stream and the heat required for evaporation is taken from the hot air stream [10]. Therefore, the heat and mass transfer characteristics across the membrane are affected [11]. For low temperature differences across the membrane, effects of the adsorption heat are negligible when analysing the heat and mass transfer across the membrane [11,12]. Fig. 2 shows the current simplified energy recovery process which is based on the assumption of neglecting the adsorption heat. Therefore, heat and moisture transportation from the hot and humid stream to the membrane surface is achieved by convection. Consequently, conduction of heat and diffusion of moisture take place through the porous membrane. Finally, heat and moisture are then transported by convection from the membrane surface to the cold and less humid stream. The whole process causes a decrease in

* Corresponding author. Address: Mechanical Engineering Department, Prince Mohammad Bin Fahd University, PO Box 1664, AlKhobar 31952, Saudi Arabia. Tel.: +966 3 8499765; fax: +966 3 8964566.

E-mail address: rafat@unswalumni.com (R. Al-Waked).

0196-8904/$ - see front matter
http://dx.doi.org/10.1016/j.enconman.2013.05.038

Nomenclature

C_p	specific heat (J kg^{-1} K^{-1})
D	diffusion coefficient (m^2 s^{-1})
E	mechanical energy (J kg^{-1})
h	enthalpy (J kg^{-1})
H	total enthalpy (J kg^{-1})
h_{fg}	enthalpy of evaporation (J kg^{-1})
J	diffusion flux (kg m^{-2})
k	thermal conductivity (W m^{-1} K^{-1})
K_{Lc}	friction factor for contracting flow
K_{Le}	friction factor for expanding flow
M_w	molecular weight (kg mol^{-1})
$\dot{m}$	mass flow rate (kg s^{-1})
P	pressure (Pa)
P_{op}	operating pressure (Pa)
q_h	sensible heat flux (W m^{-2})
R	universal gas constant (J K^{-1} mol^{-1})
S_ϕ	source term
T	temperature (K)
v	velocity (m s^{-1})
$\hbar\dot{V}$	volumetric flow rate (m^3 h^{-1})
x, y, z	Cartesian coordinates
Y_i	mass fraction of each species (kg kg^{-1})

Greek letters

ΔP	pressure drop (Pa)
ε	effectiveness (%)
ϕ	variable quantity (1, U, V, W, T, Y_v)
Γ_ϕ	diffusion coefficient of variable quantity ϕ
ω	humidity ratio (kg kg^{-1})
ρ	density (kg m^{-3})

Subscripts

a	air
c	cold
h	hot
i	inlet, species index (dry air or vapour)
l	latent
m	membrane
ma	mixed air
o	outlet
s	stream
t	total
v	vapour

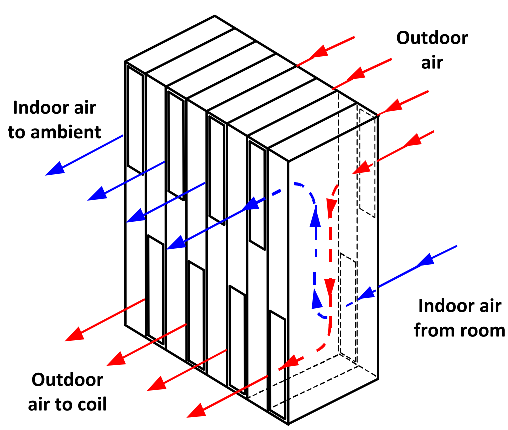

Fig. 1. Membrane (enthalpy) heat exchanger hybrid-flow configuration [1].

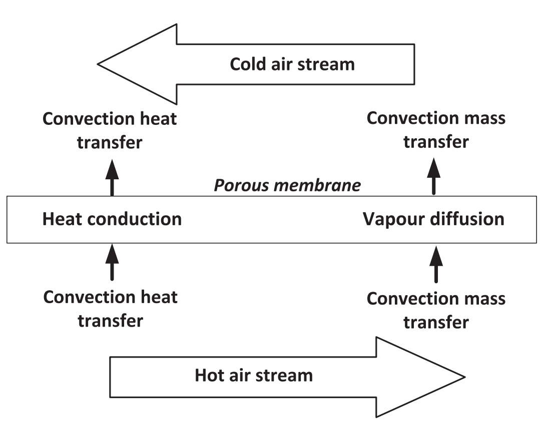

Fig. 2. Heat and moisture transfer in a membrane heat exchanger.

temperature and humidity of the supply hot and moist air stream before it enters the cooling coil.

Significant experimental, numerical and analytical research work was undertaken in the last decade to improve the performance of the enthalpy heat exchanger [9,13–15]. Experimental investigation is considered costly and time consuming [8,16,17]. Alternatively, researchers have focused their work on developing mathematical models and computer simulation codes such as Computational Fluid Dynamics (CFD) simulation to predict heat exchanger performance [4,18–20].

Available commercial CFD packages, such as FLUENT [21], suffer from limitations when it comes to modelling moisture diffusion across a porous boundary similar to the membrane heat exchanger. Heat transfer problems are well developed and solved by FLUENT [21]. Solutions for mass transfer problems are still under development, especially through membranes or porous materials [4,11]. These problems make it difficult to model the complete process of heat and mass transfer within any membrane heat exchanger. To overcome these limitations, researchers have developed in-house CFD/numerical codes, modified related inputs to the utilised CFD model or wrote user defined functions that have been implemented in CFD commercial packages such as FLUENT [21].

Zhang [20] worked on membrane-based total heat exchanger and provided fundamental data for future engineering applications. He conducted experimental work on a quasi-counter flow heat exchanger and presented the heat exchanger effectiveness as a function of air flow rates. Zhang [20] also presented a CFD model, utilising FLUENT [21], based on non-dimensional values of temperature, pressure and humidity ratios. He reported a final uncertainty value of 4.5% for sensible and latent effectiveness. In his CFD model, the mass transfer problem was solved by adopting the heat-mass transfer analogy. Zhang [20] deliberately changed the values of Prandtl number (Pr) and thermal diffusion to be the same as Schmidt number (Sc) and mass diffusion, respectively. In this way, Zhang [20] transformed his conjugate mass transfer problem to a conjugate heat transfer problem.

Min and Su [22] developed a mathematical model to analyse heat and mass transfer in the core of a membrane-based enthalpy exchanger. They have also derived equations for evaluating the thermal and moisture resistances. In their model, the physical properties of flowing air and the membrane were assumed to be constant and Lewis number (Le) was assumed to have a constant value of 0.85. The heat conduction and vapour diffusion in the two air streams were assumed to be negligible in comparison to the bulk convection. In their work, Min and Su [22,23] used vapour density difference as the moisture transfer driving force. Later on, Min and Su [24] modified their approach in utilising the humidity ratio difference as the driving force. They concluded that the thermal conductivity of the membrane has an insignificant influence on all forms of effectiveness: latent, sensible and total.

Yaïci et al. [4] presented a two-dimensional CFD model of the conjugate heat and mass transfer of parrallel-/counter flow membrane heat exchanger under typical Canadian summer and winter conditions. In their study, they adopted constant air physical properties and ignored the heat resulting from species diffusion into the air streams. Their findings were in compliance with previous research work. Furthermore, they stressed that CFD approach has proven to be both a practical and an effective design tool of HRV/ERV systems.

Nasif et al. [18] utilised FLUENT [21] to model Z-flow configuration enthalpy heat exchanger in an effort to investigate temperature and moisture distribution in the heat exchanger. They modelled moisture transfer through porous materials by developing a non-dimensional sensible-latent effectiveness ratio to obtain the moisture boundary conditions on the heat exchanger surface. They highlighted that determining the sensible-latent effectiveness ratio can only be obtained from effectiveness measurements.

The current work presents a CFD model capable of modelling the heat and mass transfer processes across the membrane within the heat exchanger using FLUENT [21]. A mesh independence study is conducted and followed by the validation of the current CFD model against published data [20]. Furthermore, effects of flow direction at the inlet of the heat exchanger on its effectiveness are examined. Simulation results are presented and analysed in terms of sensible and latent effectiveness and pressure drop across the membrane heat exchanger.

2. CFD model

The commercial CFD package, FLUENT [21], is used to simulate the heat and moisture transfer inside the membrane heat exchanger. A three-dimensional CFD pressure based solver, steady-state model of the heat exchanger is developed using the pre-processor GAMBIT software [25]. Two types of mesh elements are used: structured mesh is used to build the counter-, cross-, and parallel-flow configurations CFD model and hybrid mesh is used to build the quasi-flow configuration CFD model. The volumetric species transport model is adopted to describe the H_2O and air gas mixture with the inclusion of inlet diffusion and diffusion energy source options. The semi implicit method for pressure linked equation (SIMPLE) algorithm is employed for the calculation of pressure and velocity fields. Third order MUSCAL discretization scheme is used with momentum, energy, and species equations. Moreover, the second order upwind discretization scheme is used with the pressure model [21].

The CFD model consists of one flow passage for the hot stream and another for the adjacent cold stream. Only half of each flow passage volume is modelled on each side of the membrane surface and symmetry boundary conditions were used as shown in Fig. 3.

The membrane heat exchangers adopted in this investigation have the same dimensions and properties as those investigated by Zhang [20]. The quasi-counter flow heat exchanger is detailed by Fig. 3 and Table 1.

2.1. Assumptions

The in-house developed user defined function utilised in the current CFD model is limited by the following assumptions:

- Steady state processes of heat and mass transfer.
- The adsorption of water vapour on and from the membrane is in a dynamic equilibrium state.
- Constant and equal heat of vaporisation and heat of sorption.
- Constant and isotropic heat and mass transfer resistance through the membrane. According to Min et al. [11,12,22], heat transfer resistance is function of latent-to-sensible heat ratio. This is because the adsorption heat at the membrane surface also transfers across the membrane. However, they concluded that the thermal resistance accounts for a small fraction of the total thermal resistance and can be ignored. Furthermore, the mass transfer resistance is strongly affected by membrane properties and operating conditions [1,11,12,18,19,22–24,26]. Due to validation requirements with Zhang [20], the mass transfer resistance is considered constant.
- The Reynolds number ($Re = \rho v D_h/\mu$) at the inlet of the flow passage was found to be less than 1000; therefore, the flow is assumed to be of laminar nature [20]. The hydraulic diameter (D_h) is approximated to be ($2 \times$ passage height = 8 mm) [1]. The value of Reynolds number inside the quasi heat exchanger is expected be even lower due to the expansion the cross-section of the flow passage.

2.2. Governing equations

Fundamental equations of fluid motion are based on three conservation laws: mass, momentum and energy. Additional equations are required if, for example, a fluid is composed of various chemical species with mass diffusion. Consequently, the adopted form of the incompressible steady-state air flow equation is [21]:

$$\nabla \cdot (\rho\phi \vec{V}) = \nabla \cdot (\Gamma_\phi \nabla\phi) + S_\phi \tag{1}$$

The energy equation in the current CFD model, solved by FLUENT, can be written as [21]:

$$\nabla \cdot (\vec{V}(\rho E + p)) = \nabla \cdot \left(k\nabla T - \sum_{\mathrm{i}} h_{\mathrm{i}}\vec{J}_{\mathrm{i}}\right) \tag{2}$$

where k is the thermal conductivity, T is the moist air temperature and J_{i} is the diffusion flux of species i. The two terms on the right hand side of Eq. (2) represent the energy transfer due to conduction and species diffusion, respectively. Furthermore, the mechanical energy E is defined as [21]:

$$E = h - \frac{p}{\rho} + \frac{V^2}{2} \tag{3}$$

The sensible enthalpy h is defined for incompressible fluid flow as [21]:

$$h = \sum_{\mathrm{i}} Y_{\mathrm{i}} h_{\mathrm{i}} + \frac{p}{\rho} \tag{4}$$

$$h_{\mathrm{i}} = \int_{T_{\mathrm{ref}}}^{T} c_{\mathrm{p,i}}\, dT \tag{5}$$

When solving the conservation equations for air and vapour species, FLUENT [21] predicts the local mass fraction of each species (Y_{i}) through the solution of a convection–diffusion equation for the ith species. The species conservation equation takes the following general form:

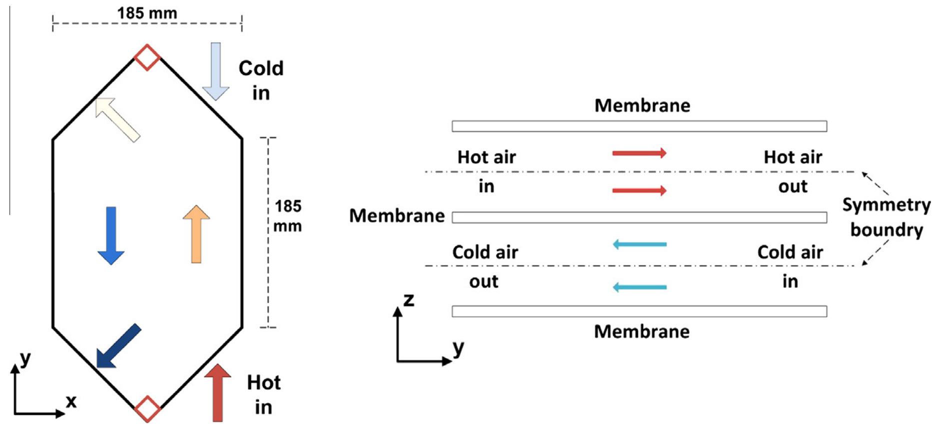

Fig. 3. Cross section of the simulated membrane heat exchanger flow passages.

Table 1
Reference values of the simulated membrane heat exchanger Zhang [20].

# Of channels	57
Membrane thickness (δ)	102 μm
Channel height	4 mm
Membrane diffusion coefficient	8×10^{-6} m^2/s
Lateral lengths (x-, y- directions)	185 mm
Membrane conductivity	0.13 W/m K
Cold air inlet temperature	27 °C
Hot air inlet temperature	35 °C
Cold air inlet relative humidity	52%
Hot air inlet relative humidity	59%

$$\nabla \cdot (\rho \vec{V} Y_{\rm i}) = \nabla \cdot \vec{J}_{\rm i} \tag{6}$$

The diffusion flux of the ith species (air or vapour) arises due to concentration gradient. By default, FLUENT [21] uses the dilute approximation, under which the diffusion flux can be written as:

$$\vec{J}_{\rm i} = -\rho D_{\rm i,ma} \nabla Y_{\rm i} \tag{7}$$

where $D_{\rm i,ma}$ is the diffusion coefficient for the ith species (air or vapour) in the moist air mixture and is defined as [27]:

$$D_{\rm a,ma} = D_{\rm v,ma} = 1.87 \times 10^{-10} \frac{T^{2.072}}{P} \tag{8}$$

The density of the utilised ideal gas law for an incompressible flow can be defined as [21]:

$$\rho = \frac{P_{\rm op}}{RT \sum \frac{Y_{\rm i}}{M_{\rm w,i}}} \tag{9}$$

where R is the universal gas constant, $M_{\rm w,i}$ is the molecular weight of air or vapour and $P_{\rm op}$ is the operating pressure which is given the value of the standard atmospheric pressure. Other properties of the moist air mixture are evaluated based on the mass weighted average of the mixture components. Furthermore, the air [28] and vapour [21] thermodynamic properties of specific heat, conductivity and viscosity are evaluated as a function of air temperature.

2.3. Boundary conditions

In order to obtain a unique solution of the governing equations (Eqs. (1), (2) and (6)), a set of boundary conditions must be provided. The boundary conditions are used to determine the arbitrary functions resulting from integrating the governing equations.

The velocity boundary condition is used to define the velocity magnitude and direction of the moist air at the hot and cold inlets of the heat exchanger. Other required inputs at this boundary are: dry-bulb temperature and vapour mass fraction.

The pressure outlet condition is used to model the flow conditions at the outlets of the heat exchanger. Required inputs into this boundary are: air gage pressure, dry-bulb temperature and vapour mass fraction. These values will be used only if there is reverse flow into the simulated domain through this boundary.

All solid surfaces of the heat exchanger, apart from the membrane, are modelled using the wall boundary condition. The no-slip condition is enforces where the air velocity magnitude is equal to zero. Similarly, no heat flux and zero diffusive flux conditions are enforced at this boundary.

At the centre of the hot and cold flow passages, the symmetry boundary condition is utilised. Symmetry boundary is usually used to reduce the extent of the computational model to symmetric subsections of the overall physical system, hence reducing computational cost. Furthermore, it is not necessary to define any parameter at this boundary. The current CFD package, FLUENT [21], enforces a zero flux of all quantities across a symmetry boundary and sets the normal velocity component at the symmetry plane to zero.

It is worth mentioning that the values used as inputs to these boundary conditions are taken from and calculated based on the quantities listed in Table 1.

2.4. Membrane modelling

The only available option for porous boundary in FLUENT [21] is the porous jump boundary which can be used to model a thin membrane. Across the porous jump boundary condition, the flow of air and related pressure drop is based on solving the Darcy equation [21]. However, this boundary does not model the mass diffusion phenomena. Alternatively, the solid thin wall boundary condition is adopted to model the membrane of the heat exchanger.

The membrane has a thickness (δ) in the order of 100 μm which makes the assumption of isotropic heat and mass transfer valid. Therefore, one-dimensional equations are accurate enough to describe the heat and mass transfer processes inside the membrane. The utilised steady-state equations of heat and mass transfer processes are [27]:

$$\frac{\partial^2 T_{\rm m}}{\partial z^2} = 0 \tag{10}$$

$$\frac{\partial^2 Y_{\rm i,m}}{\partial z^2} = 0 \tag{11}$$

In laminar flows, the fluid side heat transfer at a solid thin wall surface is computed using Fourier's law [27]:

$$q_h = -k\frac{\partial T}{\partial z}\bigg|_{hs} = -k_m\frac{\partial T_m}{\partial z}\bigg|_m = -k\frac{\partial T}{\partial z}\bigg|_{cs} \quad (12)$$

Heat transfer across the membrane is solved directly in FLUENT [21] by coupling the two sides of the membrane. The membrane conductivity, density and heat capacity are defined when defining the material properties of the heat exchanger in accordance with Table 1.

Moisture transfer at the surface of the membrane is by diffusion only because of the no-slip boundary condition. Therefore, the mass flux of water vapour at the surface can be expressed by Fick's law [27]:

$$j_v = -\rho D_{v,ma}\frac{\partial Y_v}{\partial z}\bigg|_{hs} = -\rho D_m\frac{\partial Y_{v,m}}{\partial z}\bigg|_m = -\rho D_{v,ma}\frac{\partial Y_v}{\partial z}\bigg|_{cs} \quad (13)$$

In-house user defined function (UDF) is developed to solve Eq. (13) and to provide values of vapour mass fractions at both faces of the membrane. Mass fraction values are presented according to the following equations:

$$Y_{v,mc} = Y_{v,cs} + a_1 Y_{v,hs} - a_1 Y_{v,mh} \quad (14)$$

$$Y_{v,mh} = \frac{Y_{v,cs} + (a_1 + a_2)Y_{v,hs}}{(a_1 + a_2 + 1.0)} \quad (15)$$

where a_1 and a_2 are function of the membrane physical and geometrical properties in addition to the mesh element length in the perpendicular direction.

2.5. Effectiveness

The effectiveness of a membrane heat exchanger can be presented in three different forms: sensible (ε_s), latent (ε_l) and total (ε_t) effectiveness. These parameters are calculated using the following equations [1]:

$$\varepsilon_s = \frac{\dot{m}_h c_p (T_{hi} - T_{ho}) + \dot{m}_c c_p (T_{co} - T_{ci})}{2\dot{m}_{min} c_P (T_{hi} - T_{ci})} \quad (16)$$

$$\varepsilon_l = \frac{\dot{m}_h h_{fg} (\omega_{hi} - \omega_{ho}) + \dot{m}_c h_{fg} (\omega_{co} - \omega_{ci})}{2\dot{m}_{min} h_{fg} (\omega_{hi} - \omega_{ci})} \quad (17)$$

$$\varepsilon_t = \frac{\dot{m}_h (H_{hi} - H_{ho}) + \dot{m}_c (H_{co} - H_{ci})}{2\dot{m}_{min} (H_{hi} - H_{ci})} \quad (18)$$

Due to validation needs of the current CFD model against the published experimental work of Zhang [20], the following definitions of membrane heat exchanger effectiveness were adopted [20]:

$$\varepsilon_s = \frac{(T_{hi} - T_{ho})}{(T_{hi} - T_{ci})} \quad (19)$$

$$\varepsilon_l = \frac{(\omega_{hi} - \omega_{ho})}{(\omega_{hi} - \omega_{ci})} \quad (20)$$

Values of temperatures and humidity ratios were taken from the CFD model at the inlets and outlets of the membrane heat exchanger. The presented values of the effectiveness parameters are the mass averaged values.

2.6. Energy recovered (ER)

The total amount of energy recovered as a result of installing the enthalpy heat exchanger could be simplified to the difference between total energy transferred from the hot stream to the cold stream and the energy required to overcome the additional pressure drop. For the simulated passages, energy recovered (ER) could be written as:

$$ER = \dot{m}_h (h_{hi} - h_{ho}) - \frac{\Delta P \bar{\dot{V}}}{3600} - \dot{m} v^2 (K_{Lc} + K_{Le}) \quad (21)$$

The pressure drop values across the heat exchanger (ΔP) are obtained from the CFD model, whereas values for K_{Lc} and K_{Le} are obtained from published works [29–31].

3. Results and discussion

In this section, effects of mesh element dimensions, membrane shapes and flow directions on the effectiveness of the membrane heat exchanger are presented. Validation of the current CFD model against published experimental results is detailed as well.

3.1. Effects of perpendicular distance (D_{center})

The cell centre perpendicular distance (D_{center}) from the membrane is expected to have an effect on the effectiveness (ε_s and ε_l) of the membrane heat exchanger. As listed in Table 2, six cases are investigated to show the dependence of the effectiveness on the perpendicular distance. The membrane is selected to have a square shape transfer area in which the lateral sides have the same number of mesh elements (150 elements). Furthermore, the cold and hot passages have the same number of cell elements. Counter-, cross-, and parallel-flow configurations are investigated and results are shown in Fig. 4.

Based on the proposed CFD functions, air temperature and mass fraction at the cell centre are recorded and linearly related to membrane surface values. The slope of the linear relation is dependent on the perpendicular distance between the membrane face and the adjacent cell centre. The number of elements of the hot or cold passages is listed in Table 2 and is inversely proportional to the perpendicular distance.

Variations in effectiveness values, shown in Fig. 4, ranged from 0.1% to 1.1% for sensible effectiveness and from 0.3% to 0.8% for latent effectiveness. It is noticed that counter-flow configuration has greater sensitivity to the perpendicular distance (D_{center}) followed by counter-flow configuration and last parallel-flow configuration. This is due to rapid variations in temperatures and mass fractions at the contact surfaces between the moist air cell and the membrane surface. Therefore, the smaller the distance value is the more accurate and less variant the code prediction of the value of mass fraction at the membrane surface. As shown by Fig. 4, there is no significant variation in the effectiveness when the distance value becomes less than 50 μm.

Over-estimation in values of the heat exchanger effectiveness is also been found at coarse mesh (large D_{center}) for the counter- and cross-flow configurations as shown by Fig. 4. Temperature values are read at the centre of the cell adjacent to the membrane surface by interpolating values from all other nodes of the cell. The distance of the cell centre is longer for a coarse mesh than for a fine mesh. Therefore, the temperature is expected to be colder at the cell centre in the cold stream side and hotter in the hot stream side than for a fine mesh. The same logic applies to the mass fraction at both sides of the membrane. Consequently, heat and mass transfer driving forces across the membrane tend to increase and to

Table 2
Distance of the cell centre from the membrane and the related parameters.

D_{center} (μm)	200	100	71	50	40	33
Total no. of cells ($\times 10^3$)	225	450	675	900	1125	1350
No. of elements/passage	5	10	15	20	25	30

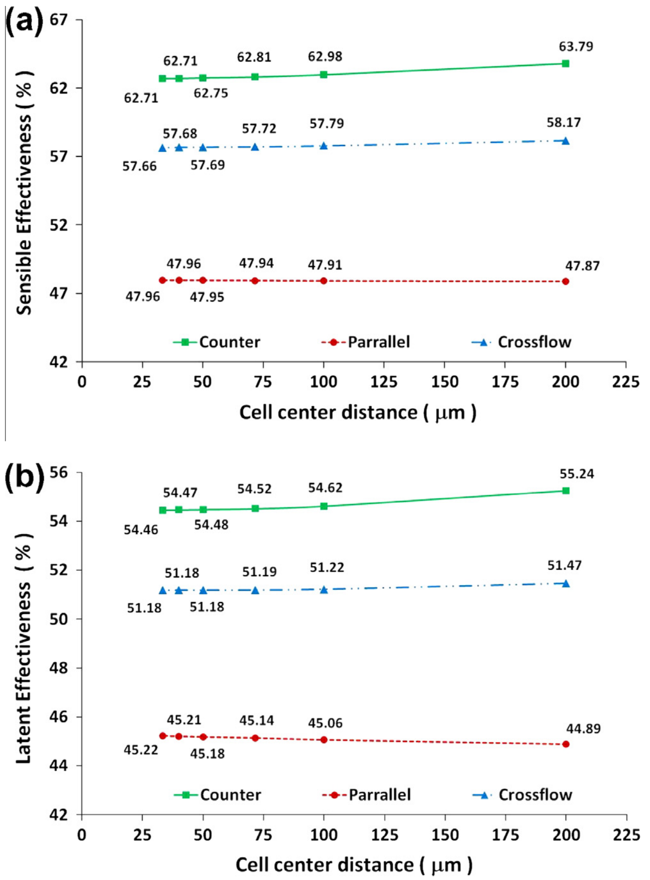

Fig. 4. Effectiveness as a function of cell centre distance from membrane surface at a volumetric flow rate of 155.8 m^3/h; (a) sensible effectiveness (ε_s), (b) latent effectiveness (ε_l).

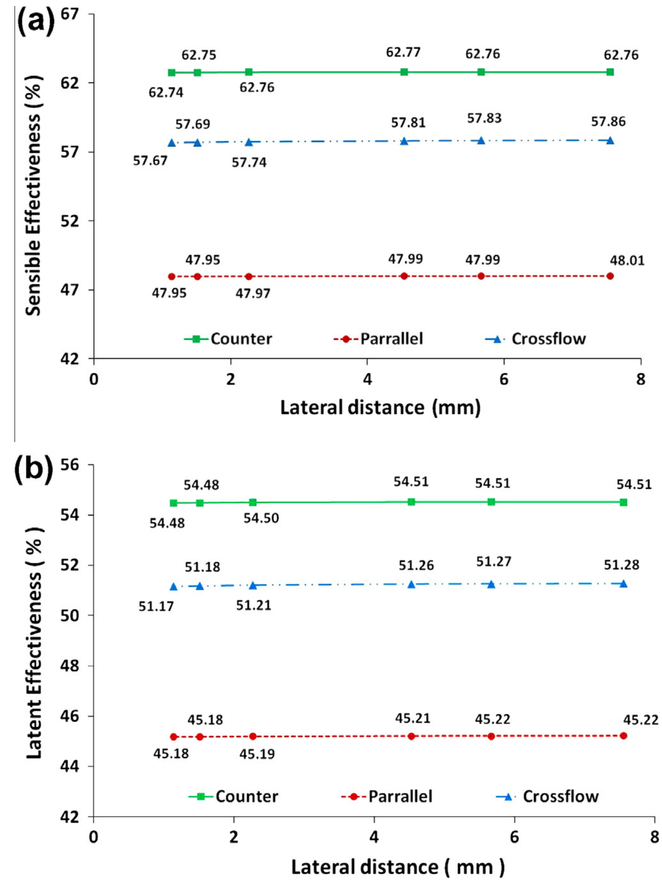

Fig. 5. Effectiveness as a function of mesh element lateral length at a volumetric flow rate of 155.8 m^3/h; (a) sensible effectiveness (ε_s), (b) latent effectiveness (ε_l).

Table 3
Mesh element length tangential to the membrane and the related number of cells.

L_{mesh} (mm)	11.33	7.55	5.66	4.53	2.27	1.51	1.13	0.91	0.76
Total no. of cells ($\times 10^3$)	16	36	64	100	400	900	1600	2500	3600
No. of elements/passage	20	30	40	50	100	150	200	250	300

contribute to the over-estimation in effectiveness values. In the parallel-flow heat exchanger, heat and mass transfer driving forces across the membrane remain at similar values. Consequently, effect of coarse/fine mesh on the effectiveness is negligible and it can be said that the performance of parallel-flow heat exchanger is insensitive to the mesh element size.

Due to the sensitivity of counter-flow configuration, dependency of effectiveness on perpendicular distance is tested further at different moist air flow rates. Similar results are obtained showing that when the perpendicular distance value is similar to the membrane thickness or less a mesh independent solution can be achieved. Therefore, a minimum of 15 mesh elements are required in the perpendicular direction of the current membrane heat exchanger for obtaining a mesh independent solution.

It can be concluded that perpendicular distance values should be in a close proximity to the membrane thickness to validate the assumption of linear dependency and to reduce the effect of convective heat and mass transfer at the surface of the membrane.

3.2. Effects of lateral mesh element length

The other aspect of mesh dependence testing is studying effects of the lateral dimensions of mesh elements. Eight cases are simulated with mesh elements length ranging from 0.76 to 11.33 mm, as listed in Table 3. The total number of cells reported in Table 3 is the sum of mesh elements in the cold and hot passages, where the cold and hot passages have the same number of elements. Both of the lateral dimensions have same values whereas the perpendicular number of elements is fixed at 20 elements.

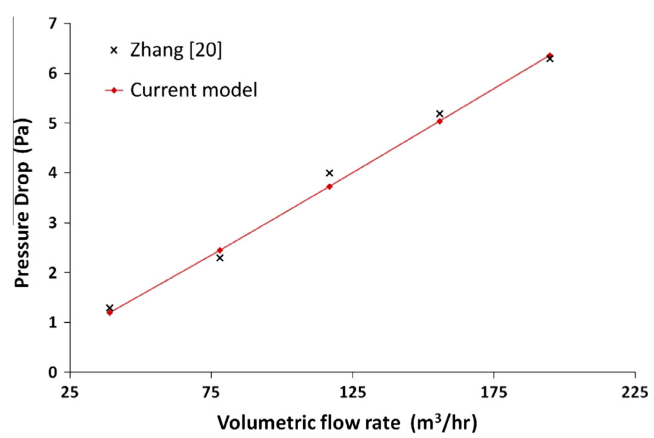

Fig. 7. Pressure drop across the membrane section of the quasi-flow heat exchanger as a function of volumetric flow rate.

It can be seen from Fig. 5 that the effectiveness of the investigated heat exchanger is not sensitive to the lateral mesh element length. The same outcome is observed for the three investigated flow configurations of counter-, cross- and parallel-flow. Therefore, the number of elements in the lateral direction should be decided

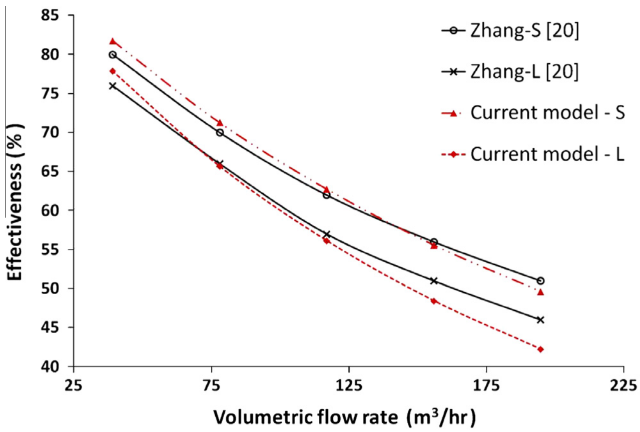

Fig. 6. Effectiveness as a function of volumetric flow rate for quasi-flow configuration.

based bounded perpendicular walls rather than the membrane boundary.

3.3. Validation of the CFD model

Based on the outcomes of mesh dependence studies presented earlier, the number of mesh elements is fixed to 15 elements in the perpendicular to the membrane direction. The number of elements in the lateral to the membrane direction is changed to accommodate changes in the shape of the heat exchanger (quasi-flow configuration) with a minimum of 120 elements. Results from the current CFD model are validated against the published results of Zhang [20] and detailed in Fig. 6 till Fig. 8.

Effectiveness of the heat exchanger decreases as the flow rate of moist air increases, as shown by Fig. 6. It also shows that both of the presented studies are in a close match. Maximum variations of 1.8% and 3.7% in sensible and latent effectiveness are noticed when results from the current CFD model and results of Zhang [20] are compared. It is worth mentioning that the current CFD model has moist air properties dependant on: temperature, pressure and composition. Furthermore, the current model simulates air as a mixture of dry air and water vapour (H_2O). However, Zhang [20] has used fixed values of conductivity and viscosity of dry air only. Effects of these discrepancies in defining moist air species and properties are shown clearly in Fig. 8.

The other parameter required to confirm the capability of the current CFD model is the pressure drop across the heat exchanger. As shown by Fig. 7, the pressure drop across the membrane section of the quasi-flow heat exchanger increases as air flow rate increases. Both of presented results show the same behaviour with minimal deviation of 0.3 Pa. Consequently, the current CFD model can be considered as a successful tool to model the complicated nature of coupled heat and mass transfer across the quasi-flow membrane heat exchanger. The advantage of presenting the true nature of moist air mixture makes the CFD model more real and enhances the applicability of obtained results with minimal or no modifications.

Differences appear when comparing the sensible effectiveness (ε_s) for the different configurations. It can be noticed that differences between results from the current CFD model and Zhang's work [20] increases as the flow rate increases to reach a maximum value of 5% for counter-flow configuration. Up to 2% of these differences are caused by the utilisation of temperature dependent moist air properties and energy sources due to species diffusion, as mentioned by Eq. (2).

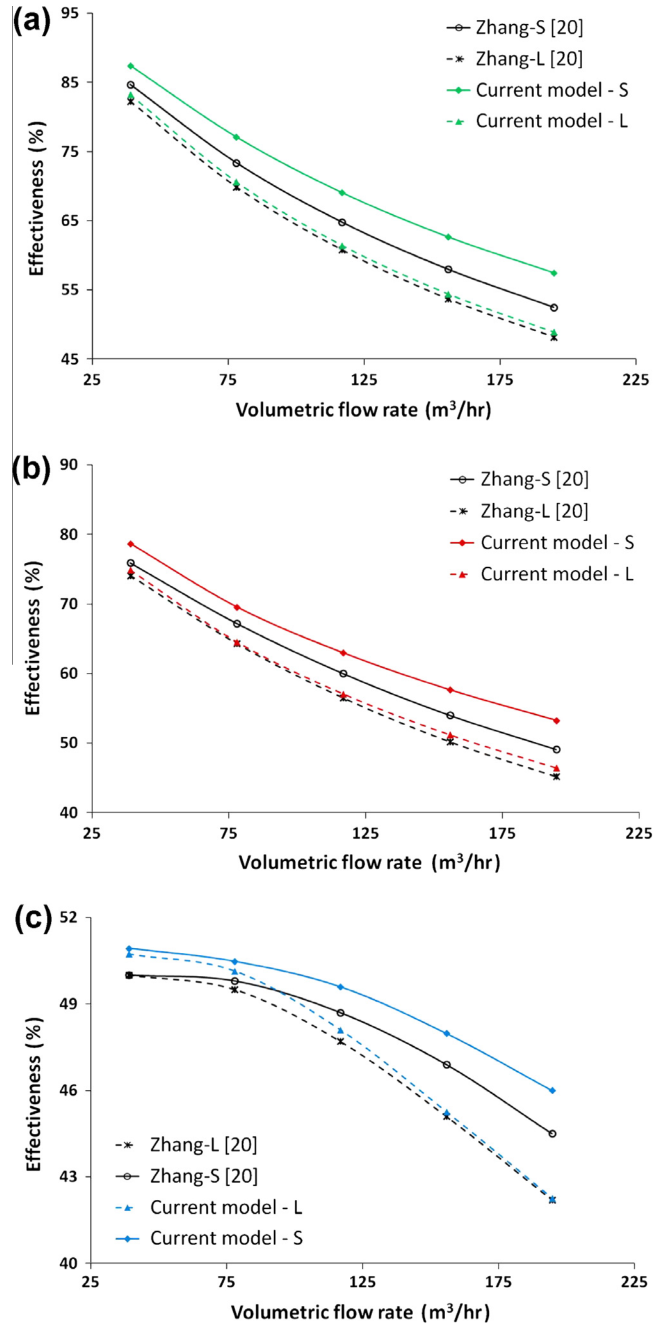

Fig. 8. Heat exchanger effectiveness at different flow configurations; (a) counter-flow, (b) cross-flow, (c) parallel-flow.

The second term on the right hand side of Eq. (2) is responsible for accommodating the air/vapour species diffusion process into the hot/cold air streams. Moist air has higher conductivity and mass diffusion values than dry air. This makes moist air a better medium for heat and mass transfer processes. Consequently, higher heat and mass exchanges between the hot and cold streams inside the heat exchanger. Therefore, the sensible heat transfer described by Eq. (2) tends to result in higher effectiveness than equations proposed by Zhang [20] for dry air with constant thermodynamic properties. As a result, the current CFD model reported higher sensible effectiveness values of the heat exchanger.

The latent effectiveness is also affected by the temperature dependent air properties and the energy source due to species diffusion. This is due to the dependence of moist air density and

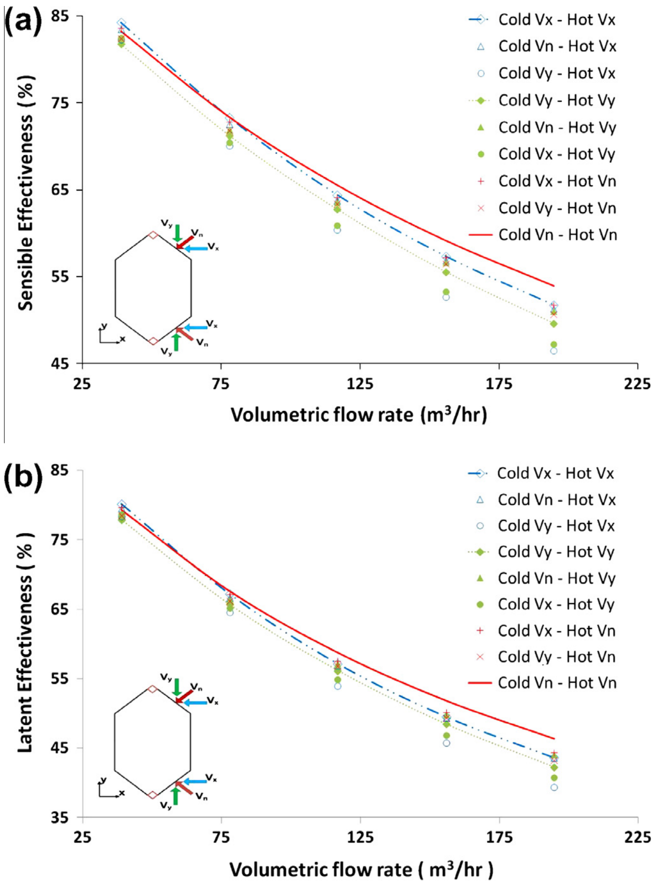

Fig. 9. Effect of inlet flow direction on heat exchanger effectiveness; (a) sensible effectiveness (ε_s), (b) latent effectiveness (ε_l).

vapour diffusivity on the moist air temperature. In turn, calculated mass fractions at the membrane surfaces are affected which affects the amount of mass transferred across the membrane. Eventually, the latent effectiveness of the heat exchanger is affected.

3.4. Effects of flow direction

Based on the configuration of quasi-flow membrane heat exchanger shown by Fig. 3, directions of inlet flow have variable effects on the flow within the heat exchanger. Therefore, a study is conducted to examine these effects and results are shown by Fig. 9 for thermal effects and Fig. 10 for pressure drop effects.

It is clear from Fig. 9 that the effectiveness of the heat exchanger (hot passage) decreases as the flow rate increases. Maximum values (ε_s and ε_l) of 84.3% and 80.2% are obtained at flow rate of 38.9 m^3/h for Cold V_x – Hot V_x flow configuration. Whereas, minimum values (ε_s and ε_l) of 46.5% and 39.4% are obtained at flow rate of 194.7 m^3/h for Cold V_y – Hot V_x flow configuration. In general, the normal-flow directions at the inlets (Cold V_n – Hot V_n) shows better performance at almost all investigated flow rates. The only exception exists for the axial flow direction (Cold V_x – Hot V_x) at flow rates of 75 m^3/h or less. All other combinations of flow configurations have less effectiveness than these two flow configurations. From thermal point of view, selecting the (Cold V_n – Hot V_n) flow configuration at the inlet would be preferable to produce the best performing heat exchanger.

The other important investigated parameter is the pressure drop across the membrane section of the heat exchanger. Results from Fig. 10 shows that the (Cold V_x – Hot V_x) flow configuration produces the greatest pressure drop. Furthermore, the

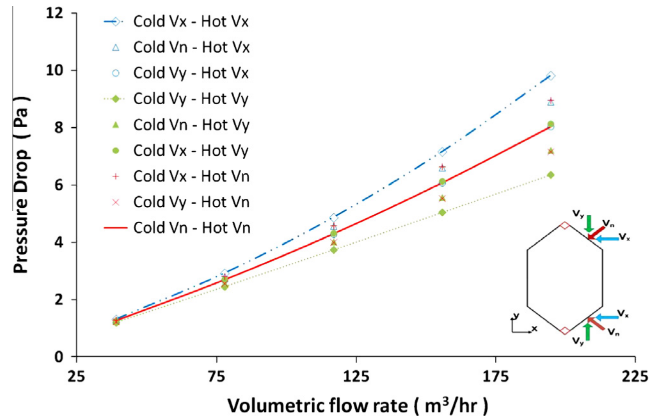

Fig. 10. Pressure drop across the membrane section at different inlet flow configurations.

(Cold V_y – Hot V_y) flow configuration produces the least pressure drop whereas all other flow configurations including the (Cold V_n – Hot V_n) flow configuration falls in between. At the highest flow rate, pressure drop under the (Cold V_x – Hot V_x) flow configuration produces as high as 1.6 times more pressure drop than the (Cold V_y – Hot V_y) flow configuration. Furthermore, the (Cold V_n – Hot V_n) flow configuration produces as high as 1.2 times more pressure drop than the (Cold V_y – Hot V_y) flow configuration. From pressure drop point of view, selecting the (Cold V_y – Hot V_y) flow configuration at the inlet would be preferable to produce the best performing heat exchanger with the least pressure drop.

Based on the previous analysis, two configurations are found to produce the best performing heat exchanger: (Cold V_n – Hot V_n) and (Cold V_y – Hot V_y) flow configurations. In order to overcome this confusion, the energy recovered from the heat exchanger (ER) is evaluated according to Eq. (21) for the investigated configurations.

The amount of energy recovered from the simulated section of the heat exchanger is presented in Fig. 11 for the fixed number of channels of 57. As little as 5.5 W per channel could be recovered at low flow rate of 38.9 m^3/h and as high as 17.5 W per channel at flow rate of 194.7 m^3/h. Results also show that the (Cold V_n – Hot V_n) flow configuration resulted in the highest quantities of energy recovered at all flow rates. On the other hand, the (Cold V_y – Hot V_x) flow configuration resulted in the lowest quantities of energy recovered at all flow rates. Although the (Cold V_y – Hot V_y) flow configuration resulted in the least pressure drop, the amount of energy recovered is not high enough when

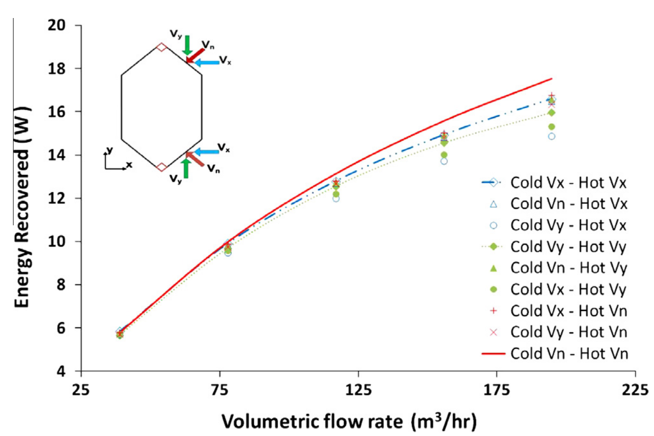

Fig. 11. Energy recovered per channel at different inlet flow configurations.

compared to those recovered from (Cold V_n − Hot V_n) flow configuration. Therefore, the (Cold V_n − Hot V_n) flow configuration is considered the best option for the investigated enthalpy heat exchanger.

4. Conclusions

A CFD model has been developed to model, simultaneously, the phenomenon of heat, mass and momentum transfer inside the enthalpy heat exchanger. The CFD model has produced reasonably accurate results when compared with an already published experimental work.

It has been noticed that counter flow configuration has greater sensitivity to the perpendicular distance from the centre of the cell to membrane surface (D_{center}) when compared to the cross- and parallel-flow configurations. To obtain accurate results, it has been found that the perpendicular distance value (D_{center}) should be in a close proximity to the membrane thickness. Furthermore, the perpendicular distance (D_{center}) has strong effect on the thermal effectiveness of the enthalpy heat exchanger. Therefore, a mesh independent solution must be sought before conducting any related parametric study. On the other hand, the lateral mesh element length has been found to have minimal effect on the thermal effectiveness of the enthalpy heat exchanger.

For the quasi heat exchanger, it has been found that the flow direction at the inlet section of the membrane heat exchanger affects the thermal performance. It has been found that selecting the (Cold V_n − Hot V_n) flow configuration at the inlet would be preferable to produce the best performing heat exchanger.

References

[1] Nasif MS. Analysis and modelling of membrane heat exchanger in hvac energy recovery systems. PhD thesis in Mechanical Engineering. University of New South Wales, Sydney; 2006. p. 245.
[2] El Fouiha Y, Stabat P, Rivière P, Hoang P, Archambault V. Adequacy of air-to-air heat recovery ventilation system applied in low energy buildings. Energy Build 2012;54:29–39.
[3] Zhang LZ, Niu JL. Energy requirements for conditioning fresh air and long-term savings with a membrane-based energy recovery ventilator in Hong Kong. Energy 2001;26:119–35.
[4] Yaïci W, Ghorab M, Entchev W. Numerical analysis of heat and energy recovery ventilators performance based on CFD for detailed design. Appl Therm Eng 2013;51:770–80.
[5] Liu J, Li W, Liu J, Wang B. Efficiency of energy recovery ventilator with various weathers and its energy saving performance in a residential apartment. Energy Build 2010;42:43–9.
[6] Al-Rabghi OM, Akyurt MM. A survey of energy efficient strategies for effective air conditioning. Energy Convers Manage 2004;45:1643–54.
[7] Yau YH, Ng WK. A comparison study on energy savings and fungus growth control using heat recovery devices in a modern tropical operating theatre. Energy Convers Manage 2011;52:1850–60.
[8] Fernandez-Seara J, Diz R, Dopazo A, Ferro JM. Experimental analysis of an air-to-air heat recovery unit for balanced ventilation systems in residential buildings. Energy Convers Manage 2011;52:635–40.
[9] Mardiana-Idayu A, Riffat SB. Review on heat recovery technologies for building applications. Renew Sustain Energy Rev 2012;16:1241–55.
[10] Liu S, Riffat S, Zhao X, Yuan Y. Impact of adsorbent finishing and absorbent filming on energy exchange efficiency of an air-to-air cellulose fiber heat & mass exchanger. Build Environ 2009;44:1803–9.
[11] Min JC, Wang L. Coupled heat and mass transfer during moisture exchange across a membrane. J Membr Sci 2013;430:150–7.
[12] Min JC, Wang LN. Heat of adsorption and its effect on transmembrane heat transfer. J Membr Sci 2012;409–410:173–9.
[13] Liu D, Zhao FY, Tang GF. Active low-grade energy recovery potential for building energy conservation. Renew Sustain Energy Rev 2010;14:2736–47.
[14] Chua KJ, Chou SK, Yang WM, Yan J. Achieving better energy-efficient air conditioning – a review of technologies and strategies. Appl Energy 2013;104:87–104.
[15] Zhang LZ. Progress on heat and moisture recovery with membranes: from fundamentals to engineering applications. Energy Convers Manage 2012;63:173–95.
[16] Mardiana-Idayu A, Riffat S. An experimental study on the performance of enthalpy recovery system for building applications. Energy Build 2011;43:2533–8.
[17] Liang CH, Zhang LZ, Pei LX. Independent air dehumidification with membrane-based total heat recovery: modeling and experimental validation. Int J Refrigeration 2010;33:398–408.
[18] Nasif MS, Al-Waked R, Behnia M, Morrison G. Air to air enthalpy heat exchanger. Heat Transfer Eng 2012;33:1–15.
[19] Nasif MS, Al-Waked R, Morrison G, Behnia M. Membrane heat exchanger in HVAC energy recovery systems: systems energy analysis. Energy Build 2010;42:1833–40.
[20] Zhang LZ. Heat and mass transfer in a quasi-counterflow membrane-based total heat exchanger. Int J Heat Mass Transfer 2010;53:5478–86.
[21] FLUENT Incorporated. FLUENT user's guide version 6.3. Lebanon, New Hampshire, USA; 2006.
[22] Min JC, Su M. Performance analysis of a membrane-based enthalpy exchanger: effects of the membrane properties on the exchanger performance. J Membr Sci 2010;348:376–82.
[23] Min JC, Su M. Performance analysis of a membrane-based energy recovery ventilator: effects of the membrane spacing and thickness on the ventilator performance. Appl Therm Eng 2010;30:991–7.
[24] Min JC, Su M. Performance analysis of a membrane-based energy recovery ventilator: effects of outdoor air state. Appl Therm Eng 2011;31:4036–43.
[25] FLUENT Incorporated. GAMBIT users guide version 2.4. Lebanon, New Hampshire, USA; 2006.
[26] Zhang LZ, Liang CH, Pei LX. Heat and moisture transfer in application scale parallel-plates enthalpy exchangers with novel membrane materials. J Membr Sci 2008;325:672–82.
[27] Cengel YA. Heat and mass transfer: a practical approach. 3rd ed. Singapore: McGraw-Hill; 2006.
[28] Kroger DK. Air-cooled heat exchangers and cooling towers. Tulsa, USA: PennWell Corp.; 2004.
[29] Çengel YA, Cimbala JM. Fluid mechanics: fundamentals and applications. 2nd ed. McGraw-Hill; 2010.
[30] Munson BR, Young DF, Okiishi TH. Fundamentals of fluid mechanics. 6th ed. Wiley & Sons; 2010.
[31] Fox RW, McDonald AT, Pritchard PJ. Introduction to fluid mechanics. 8th ed. Wiley & Sons; 2010.